

Research Paper

CO₂ bubbling-based 'Nanobomb' System for Targetedly Suppressing Panc-1 Pancreatic Tumor via Low Intensity Ultrasound-activated Inertial Cavitation

Kun Zhang^{1,2}, Huixiong Xu², Hangrong Chen¹,, Xiaoqing Jia¹, Shuguang Zheng², Xiaojun Cai¹, Ronghui Wang³, Juan Mou¹, Yuanyi Zheng³, and Jianlin Shi¹,

1. State Key Laboratory of High Performance Ceramics and Superfine Microstructures, Shanghai Institute of Ceramics, Chinese Academy of Sciences, 1295 Ding-Xi Road, Shanghai 200050, P. R. China.
2. Department of Medical Ultrasound, Shanghai Tenth People's Hospital, Tongji University School of Medicine, 301 Yan-chang-zhong Road, Shanghai, 200072, P. R. China.
3. Second Affiliated Hospital of Chongqing Medical University, 76 Linjiang Road, Yuzhong District, Chongqing 400010, P. R. China.

 Corresponding authors: Hangrong Chen and Jianlin Shi, State Key Laboratory of High Performance Ceramics and Superfine Microstructures, Shanghai Institute of Ceramics, Chinese Academy of Sciences, 1295 Ding-Xi Road, Shanghai 200050, P. R. China, Fax: 86-21-52413122; Tel:86-21-52415305; E-mail: hrchen@mail.sic.ac.cn, jlshi@sunm.shcnc.ac.cn; Yuanyi Zheng, Second Affiliated Hospital of Chongqing Medical University, 76 Linjiang Road, Yuzhong District, Chongqing 400010, P. R. China, Fax:86-23-15213318371; Tel:86-23-63809074; E-mail: zhengyuanyi@gmail.com

© 2015 Ivyspring International Publisher. Reproduction is permitted for personal, noncommercial use, provided that the article is in whole, unmodified, and properly cited. See <http://ivyspring.com/terms> for terms and conditions.

Received: 2015.05.14; Accepted: 2015.08.05; Published: 2015.09.12

Abstract

Noninvasive and targeted physical treatment is still desirable especially for those cancerous patients. Herein, we develop a new physical treatment protocol by employing CO₂ bubbling-based 'nanobomb' system consisting of low-intensity ultrasound (1.0 W/cm²) and a well-constructed pH/temperature dual-responsive CO₂ release system. Depending on the temperature elevation caused by exogenous low-intensity therapeutic ultrasound irradiation and the low pH caused by the endogenous acidic-environment around/within tumor, dual-responsive CO₂ release system can quickly release CO₂ bubbles, and afterwards, the generated CO₂ bubbles waves will timely explode before dissolution due to triggering by therapeutic ultrasound waves. Related bio-effects (e.g., cavitation, mechanical, shock waves, etc) caused by CO₂ bubbles' explosion effectively induce instant necrosis of panc-1 cells and blood vessel destruction within panc-1 tumor, and consequently inhibit the growth of panc-1 solid tumor, simultaneously minimizing the side effects to normal organs. This new physiotherapy employing CO₂ bubbling-based 'nanobomb' system promises significant potentials in targetedly suppressing tumors, especially for those highly deadly cancers.

Key words: Nanobomb, inertial cavitation, low intensity ultrasound, panc-1 pancreatic cancer, dual-responsive CO₂ release

Introduction

In the chemotherapeutics of tumors, some of inevitable drawbacks, such as poor selectivity and high cost of anticancer drugs, great suffering or side effects to patients, multidrug resistance and cancer reoccurrence, remain challenging to date [1]. To overcome these problems, many physical treatment protocols, have been developed to effectively and

safely eradicating tumors [2-11], and ultrasound treatment is the typical one, because ultrasound can provide much larger penetration depth to treat deep-seated tumors. Additionally, it also possesses some other inspiring merits, e.g., noninvasive and local treatment, independence of the types of tumors and universality. Therefore, ultrasound treatment is

especially applicable for those deadly tumors, such as panc-1 pancreatic solid tumor of high lethality and invasiveness.

At present, the common ultrasound treatment is high intensity focused ultrasound (HIFU) [12], nevertheless high power density (generally above 10^5 W/cm²) in HIFU treatment usually results in the burns of normal organs or tissues along the acoustic channels [2-4]. Therefore, it is expected that easily accessible low-intensity ultrasound (LIU, power density: below 2 W/cm²) that is commonly used in clinical sonophoresis of drug [13], will be a promising treatment method applicable for those high lethal cancers, *e.g.*, panc-1 pancreatic cancer, especially under the assistance of artificial cavitation nuclei [14]. When employing inertial cavitation to promote cancer ultrasound treatment, two crucial problems should be addressed. One is how to induce bubbles, which is also the precondition for the successful ultrasound treatment. Fortunately, multiple localized and exogenous triggers (light, electricity, magnetic field and ultrasound) and endogenous triggers (pH and enzyme) have been well designed to control releases of drug, gene or other molecules [15-19], which can provide experiences for designing smart artificial cavitation nuclei. The other problem is how to induce the explosion (inertial cavitation) of the bubbles, which is extremely pivotal especially for those water-soluble free gas bubbles, *e.g.*, CO₂ bubbles, because such water-soluble free bubbles would rapidly vanish in blood circulation without excitation [14,20].

Herein, a novel dual-responsive CO₂ release system consisting of hollow mesoporous silica nanoparticles (HMSNs) carrier and L-arginine (LA) capable of adsorbing and producing CO₂ bubbles in response to pH and/or temperature has been engineered. The design concept of such a responsive CO₂ release system was primarily originated from the reversible adsorption/desorption reaction of CO₂ by LA molecules that is sensitive to pH value and/or temperature variations. A very low intensity ultrasound (1.0 W/cm²) was used as trigger to safely and locally generate hyperpyrexia and shock waves to trigger generation and instant explosion of CO₂ bubbles, respectively. Especially, a highly lethal and rare-reported tumor cancer, panc-1 human pancreatic, was employed as the tumor model.

As a concept of proof, a large amount of CO₂ bubbles have been demonstrated to burst from the CO₂ release system, which instantly explode to induce the necrosis of tumor cells *via* occluding the blood supply, and consequently inhibit the growth of panc-1 pancreatic solid tumor both *in vitro* and *in vivo* under the stimulations of two local triggers, *i.e.*, acidic environment around tumor (endogenous trigger) and ul-

trasound irradiation (exogenous trigger). More importantly, absences of acidity and therapeutic ultrasound irradiations in normal organs as well as the rapid dissolution property of CO₂ bubbles can avoid damages to normal organs or tissues [20]. On the contrary, in tumor region, the applied ultrasound irradiation can not only induce generation of CO₂ bubbles, but also timely trigger explosion (inertial cavitation) of CO₂ bubbles before their dissolution. Assuredly, such a CO₂ bubbling-based 'nanobomb' system is highly promising for the extensive applications in the targeting therapies of many tumors without arousing agony of patients due to its locally responsive explosion and independence of the types of tumors.

Materials and Methods

In vivo ultrasound imaging

All animal experiments in this manuscript were performed according to protocols approved by the Laboratory Animal Center of Shanghai Tenth Peoples' Hospital and were in accordance with the policies of National Ministry of Health. Herein, VX-2 tumor-bearing New Zealand rabbit as models to investigate the lifetime of CO₂ bubbles without US irradiation and ultrasound-triggered *in vivo* explosion of CO₂ bubbles, and CO₂ bubble dispersion was obtained from receiving upper solution of Video S4. When investigating the lifetime of CO₂ bubbles, after intratumorally injecting CO₂ bubbles, at different timing points, ultrasonic images were captured. When investigating ultrasound-triggered *in vivo* explosion of CO₂ bubbles, before and after therapeutic ultrasound irradiation, diagnostic ultrasonic images were captured, and after injecting CO₂ bubbles, therapeutic ultrasound irradiation was instantly enforced. The *in vivo* ultrasound imaging was performed on Philips IU22.

In experiments of employing HMSN-LA-CO₂ for inhibiting the growth of panc-1 xenograft solid tumor, before and after intravenous injection of HMSN-LA-CO₂ (0.1 ml, dose: 10 mg/ml HMSN) and subsequent therapeutic ultrasound irradiations, diagnostic ultrasound imaging for tumor was performed, and images were recorded by Philips IU22. The therapeutic ultrasound irradiations were conducted on a portable ultrasound therapeutic apparatus (Chattanooga, USA) with 1 MHz transducer of 1 cm in diameter under 1.0 W/cm²-20%, and all. In order to observe CO₂ bubbles *in vivo* in tumor, 808 nm laser (1.2 W/cm², 30 s) was employed to heat HMSN-LA-CO₂ and BFI and CHI modes were employed, and GE LogiQ E9 system with a 8 MHz transducer was employed.

Inhibitory capability of HMSN-LA-CO₂ for the growth of panc-1 xenograft solid tumor on nude mice model

Panc-1 pancreatic solid tumor-bearing nude mice (36 in sum, and averaged into 6 groups corresponding to Control, US, HMSN-LA, US+LA-CO₂, HMSN-LA-CO₂ and US+HMSN-LA-CO₂), weighing 18-22 g were supplied by Laboratory Animals Center of Shanghai Tenth Peoples' Hospital, China. All the samples (HMSN dose: 50 mg/Kg, HMSN-LA dose: 62.5 mg/Kg) with the same particle concentration were injected *via* tail vein. After perfusion, the tumor tissues were radiated for 12 cycles of irradiations per day on portable ultrasound therapeutic apparatus (Chattanooga, USA), and the parameter of each cycle is 1.0 MHz-1.0 W/cm²-20 %-122 KPa for 15 s with a 60 s interval of each cycle. Between tumors and therapeutic US transducer, the sound-absorbing panel with a hole whose diameter corresponds to tumor size was added. Such irradiations were carried out every day, and photographing of tumors and tumor volume measurements were also implemented every day. At the 18th day, the nude mice were executed, and tumor and other organs (heart, liver, spleen, lung and kidney) of each nude mouse were isolated for staining with hematoxylin and eosin (H&E) and CD34 immunohistochemical for histopathological analysis by optical microscope, and additionally, the tumors are stained by tunnel immunofluorescence staining for detecting the apoptosis cells and western blot analysis of related protein was simultaneously carried out. Additionally, normal organs were also stained by hematoxylin and eosin (H&E) and CD34 immunohistochemical for histopathological analysis by optical microscope.

ICP quantifying the distributions of HMSN-LA-CO₂ in different organs

Panc-1 pancreatic solid tumor-bearing nude mice (36 in sum, and averaged into 6 groups), weighing 18-22 g were supplied by Laboratory Animals Center of Tenth Peoples' Hospital of Tongji University. The experiment was approved ethically and scientifically by Tongji University, and complied with Practice for Laboratory Animals in China. All the samples (HMSN dose: 50 mg/Kg, HMSN-LA dose: 62.5 mg/Kg) were injected *via* tail vein. After intravenously injecting HMSN-LA-CO₂, the 1st and 2nd groups were regarded as control without US irradiation; the 3rd and 4th groups experienced with US-1 irradiation and the 5th and 6th groups experienced US-2 irradiation. At 4 h later, the nude mice in the 1st, 3rd and 5th groups were executed, and tumor were taken out and dissolved for ICP measurement. At 12 h later, the nude mice in other groups (2nd, 4th and 6th) were executed, and tu-

mor were taken out and dissolved for ICP measurement. US-1: before injecting HMSN-LA-CO₂, the nude mice was radiated by ultrasound, and the irradiation method is pulsed (irradiation time is 15 s, the interval is 60 s and the cycle is 6). US-2: repeated US-1 before injecting HMSN-LA-CO₂ and at the beginning of each hour after injecting HMSN-LA-CO₂, and the number of repetition round is 4.

As for evaluation on bio-distribution of Si elements without ultrasound irradiation to determine when to start ultrasound irradiation, after intravenously injecting HMSN-LA-CO₂, at different certain timing points, the nude mice were executed, and tumor and other normal organs were taken out and dissolved for ICP measurement.

Results and Discussion

Design and construction of dual-responsive CO₂ release system (HMSN-LA-CO₂)

Owing to high surface area and excellent biocompatibility [21], HMSNs have been widely reported as drug carriers in the biomedicine field [22-24]. The well-defined HMSNs with a particle size of around 300 nm (Figure S1_{g1,g2} and Figure 1a,b) were fabricated *via* well-regulating the dynamic competition process between etching and re-growth (CPER) [25], and employed as carriers to construct such a dual-responsive CO₂ release system. Noticeably, such a method can also be extended to fabricate many other nanostructures (Figure S1).

Figure 2 shows the whole design concept and synthetic route of such a CO₂ bubbling-based 'nanobomb' system. Substantial amount of LA molecules are firstly loaded within HMSNs carriers *via* hydrogen bonding (between Si-OH and -NH₂) and electrostatic interaction, which is proved by comparing zeta potentials and size distribution between HMSN and HMSN-LA (Figure 1g and Figure S2). Reductions in surface area and pore diameter (Figure 1c,d) and emergence of characteristic peaks (Figure 1f) of LA at 1505 cm⁻¹, 1670 cm⁻¹ and 1454 cm⁻¹ after loading LA molecules demonstrate the successful loading of LA [26], and the loading amount is *cal.* 20% *via* TG analysis (Figure 1e). More importantly, no evident agglomeration is observed in Figure S3, indicative of excellent stability of HMSN-LA in both SBF and serum.

Since each LA molecule contains one guanidino group that is consisted of one primary amine group and two secondary amine groups, the guanidino group (pKa: 12.48) is the strongest basic group beneficial for chemically adsorbing acidic CO₂ gaseous molecules [27,28], determining that LA can be regarded as one of the best candidates capable of ad-

sorbing CO₂. As indicated in Figure 2A and 2D, two products including unstable carbamate and metastable bicarbonate can be generated after reaction between LA and CO₂, yielding HMSN-LA-CO₂ [29-31]. In FTIR spectra (Figure 1f), a new characteristic peak at 2978 cm⁻¹ (N⁺-H stretching vibration) of HMSN-LA-CO₂ suggests the successful CO₂ chemical adsorption. Additionally, the successive increase of

Zeta potential from HMSN to HMSN-LA, and finally to HMSN-LA-CO₂ also confirms the successful adsorption of CO₂ (Figure 1g) [32]. Noticeably, the accumulative release amount of LA molecules from HMSN-LA-CO₂ dispersed in SBF solution is still less than 20 % even at pH=4.5 (Figure S4), demonstrating the excellent stability of HMSN-LA-CO₂.

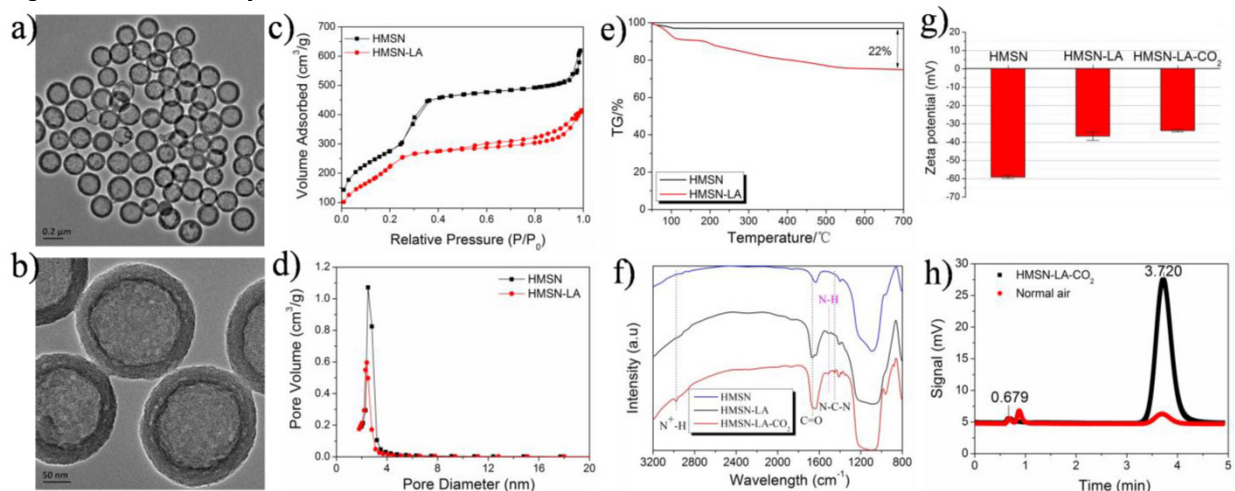


Figure 1. Characterizations of CO₂ bubbling-based nanobomb. (a,b) TEM images of HMSN-LA-CO₂, (c,d) N₂ adsorption and desorption isotherms (c) and pore diameter distributions (d) of HMSNs and HMSN-LA-CO₂; (e) TG curve of HMSN-LA; (f,g) FTIR spectra (f) and Zeta potentials (g) of HMSN, HMSN-LA and HMSN-LA-CO₂; (h) the GC-MS signals of HMSN-LA-CO₂ and normal air for characterizing CO₂, and the peak at 3.72 min represent CO₂.

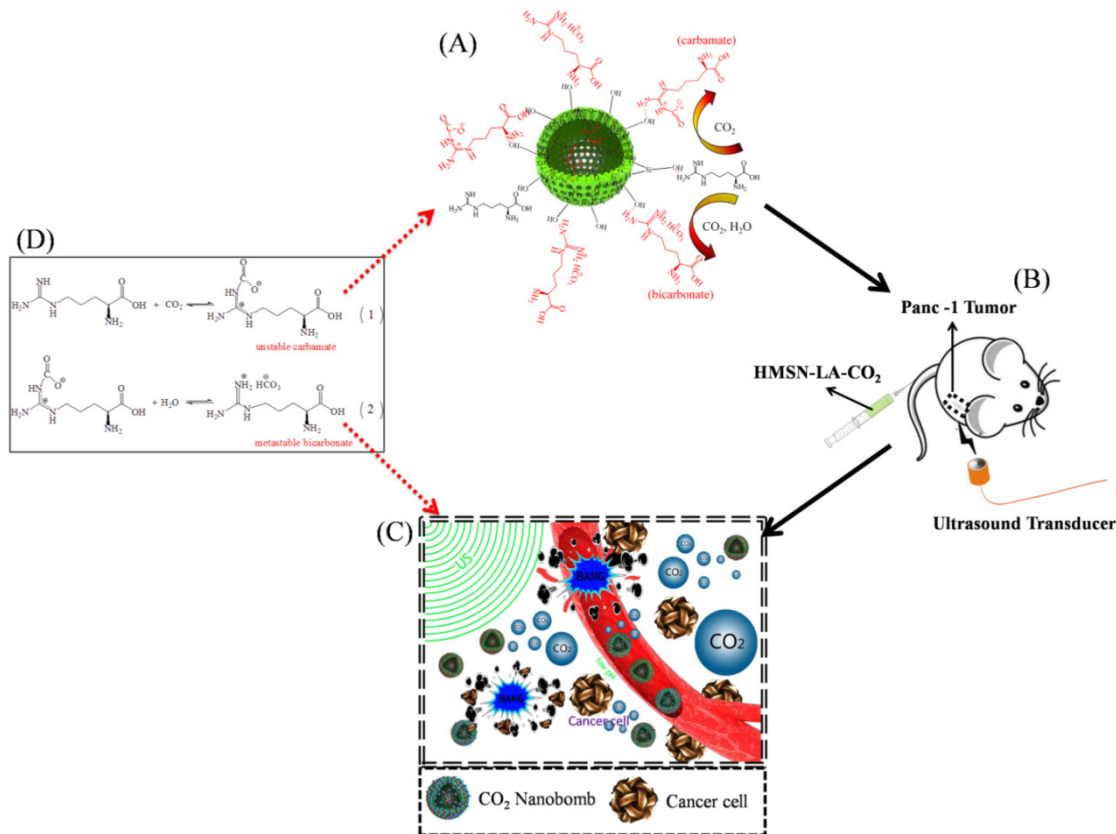


Figure 2. Technical route of CO₂ nanobomb system (US+HMSN-LA-CO₂) in inhibiting the growth of panc-1 tumor *via* explosion (inertial cavitation). (A) Schematic illustration of preparation procedure of dual-responsive CO₂ nanobomb (HMSN-LA-CO₂); (B) Therapeutic procedure of HMSN-LA-CO₂, (C) Scheme of the therapeutic mechanism of CO₂ nanobomb system, and (D) involved chemical adsorption and desorption reaction formulas of CO₂ by HMSN-LA.

pH/temperature dual-responsive release behavior of CO₂ from HMSN-LA-CO₂

Owing to the reversible and exothermic process of CO₂ adsorption [14,30], HMSN-LA-CO₂ will rapidly generate CO₂ bubbles upon raising temperature. Meanwhile, owing to the deprotonation (H⁺ production) of primary or secondary amine groups in LA during CO₂ adsorption [31], the reverse reaction (CO₂ desorption) will take place when decreasing pH value (adding exogenous H⁺) according to Le Chatelier's principle, which will also facilitate HMSN-LA-CO₂ to generate CO₂ bubbles. Gas chromatograph mass spectrometer (GC-MS) was herein employed to monitor CO₂ release by changing pH value and temperature. A more evident characteristic peak at 3.72 mV corresponding to CO₂ in comparison to air control convincingly indicates lots of CO₂ release from HMSN-LA-CO₂ (Figure 1h). The CO₂ release profile (Figure S5a₁), demonstrates HMSN-LA-CO₂ indeed possesses a pH-responsive release behavior at 37 °C, wherein higher release rate is obtained at lower pH values, and *vice versa*. Similar results can also be obtained at 50 °C or 70 °C (Figure S5a_{2,3}). Additionally, a temperature-responsive release behavior can be clearly observed *via* tuning temperature at either pH = 7.4 or 4.7 or 6.0 (Figure S5b₁₋₃). It is worth noting that the *in vitro* CO₂ release rate in GC-MS measurement is conducted using N₂ as carrier gas in an unsealed gas circuit. To investigate the release behavior of CO₂ from HMSN-LA-CO₂ in blood vessels, a mimic experiment was conducted in fresh blood without any carrier gas and, it is found that CO₂ release rate was slowed down owing to the blood pressure and protein encapsulation (Figure S6).

Furthermore, ultrasound imaging technology consisting of B fundamental imaging (BFI) and contrast harmonic imaging (CHI) modes was employed to directly monitor both the pH and temperature-dependent CO₂ release behaviors. It can be clearly found that when the temperature is raised above 50 °C or the pH value is lowered to 4.7, the domains of interest circled by the elliptical dotted line (Figure 3a_{2,2}) become much brighter than that under normal temperature and pH value (*i.e.*, 37 °C, 7.4) (Figure 3a_{1,1}), confirming the pH/temperature dual-responsive behaviors of HMSN-LA-CO₂. More convincingly, videos S1, S2 and S3 visually demonstrate pH- or temperature-responsive emergence of CO₂ bubbles, wherein no visible CO₂ bubbles occur at normal temperature and/or pH value (video S1), while CO₂ bubbles will be continuously generated once the temperature increases (video S2) or pH value is lowered (video S3). In *in vivo* level, since laser as heat source is disabled to generate mechanical waves

for triggering bubbles' explosion, 808 nm laser was employed instead of ultrasound irradiations to trigger *in vivo* production of CO₂ bubbles from HMSN-LA-CO₂. Brighter contrast under both B fundamental imaging (BFI) and contrast harmonic imaging (CHI) modes upon heating the tumor by 808 nm laser is clearly observed (Figure S7), directly demonstrating *in vivo* temperature-dependent CO₂ release from HMSN-LA-CO₂. Such a temperature-dependent CO₂ release behavior can also be demonstrated *via* optical microscopic imaging (Figure S8), wherein CO₂ bubbles immediately emerge from HMSN-LA-CO₂ dispersion in degassed PBS when the temperature was raised to 50 °C, but HMSN-LA dispersion, it failed at either room temperature or 50 °C. Additionally, more CO₂ bubbles from HMSN-LA-CO₂ dispersion in degassed PBS than that from HMSN-LA dispersion in CO₂-supersaturated PBS (Figure S8 and Figure S9) indicates HMSN-LA-CO₂ can serve as CO₂ source. Besides aforementioned direct heating to generate CO₂ bubbles, ultrasound-mediated hyperthermia could also directly promote CO₂ release from HMSN-LA-CO₂ (Figure S10).

As for the local ultrasound-triggered explosion of CO₂ bubbles, it can be clearly observed that the CO₂ bubbles will instantly explode once the produced CO₂ bubbles were exposed to local ultrasound irradiation (Figure 3c,d and video S4). Besides direct observations, the quantitative inertial cavitation dose (ICD), which is usually employed to reflect the degree of inertial cavitation, can be obtained *via* a specific instrument (Figure 3e). It is clear that higher ICD values can be obtained after raising temperature (45 °C) or/and reducing pH value (6.0) under the excitation of 1 MHz ultrasound (Figure 3f), which can be attributed to the fact that HMSN-LA-CO₂ could produce more CO₂ bubbles, and thus generate more violent explosion under higher temperature and more acidic condition. In *in vivo* evaluations, without therapeutic ultrasound irradiation, CO₂ bubbles will be gradually dissolved within 5 min in VX2 tumor implanted in New Zealand rabbit (Figure S11), while explosion of CO₂ bubbles immediately occur once ultrasound irradiation was applied (Figure S12), which sufficiently suggests that ultrasound-triggered explosion before dissolution of CO₂ bubbles is essential for cancer treatment.

***In vitro* cavitation effect of CO₂ bubbling-based 'nanobomb' system**

In order to convincingly evaluate the inertial cavitation of HMSN-LA-CO₂ triggered by therapeutic ultrasound in physically killing panc-1 cells, it is necessary to exclude the probable apoptosis interferences from ultrasound, hyperpyrexia and acidity *via* theo-

retical analysis, experimental design and experiments, parameter choice, *et al.* pH reduction-induced apoptosis can be excluded *via in vitro* experimental evaluations. In Figure 4a,b, no evident differences between with hydroxyethylpiperazine ethanesulfonic acid (HEPES) and without HEPES were observed (Figure 4a) [33-35], and no evident apoptosis occurred within 2 h at pH=6.2 (Figure 4b), indicating no pH reduction-induced apoptosis within 2 h incubation after ultrasound radiation, which was also in consistent with the previous reports [33,34].

Choosing appropriate ultrasound parameters can be employed to eliminate influences from hyperpyrexia-induced apoptosis. Herein, two groups of parameters, 0.6 W/cm² (power density)-50% (duty cycle) and 1.0 W/cm²-20% have been chosen to evaluate the treatment efficacy of CO₂ bubbles' explosion for panc-1 cells according to the evaluations in Figure S13a-c and Figure S14 and related references [36,37]. Furthermore, panc-1 cell line was a heat-resisting cell line and apoptosis would not occur within 1 h of hyperpyrexia treatment [33,38,39], which can theoretically exclude hyperpyrexia-induced apoptosis. More importantly, experimental results in Figure 4c,d confirm no hyperpyrexia-induced apoptosis.

Figure S15 displays the viability of panc-1 cell lines treated with different groups *via* MTT method, wherein HMSN-LA-CO₂ indeed performs much better than HMSN-LA, especially exposure to ultrasound irradiation (US+HMSN-LA-CO₂). However, the MTT method failed in deciding which one should be mainly responsible for the cell death, since besides CO₂ bubbling-induced instant necrosis, a fraction of effected cells could progressively generate the programmed death (apoptosis) when they were exposed to ultrasound irradiation alone or combined with microbubbles for a long time [40,41]. To exclude ultrasound-induced programmed apoptosis, more detailed tests including flow cytometry, SEM and confocal/optical microscopic observations were carried out immediately after ultrasound irradiations, since programmed apoptosis needed several hours after ultrasound irradiation [40,41].

Figure 5a shows the *in vitro* results of flow cytometry, wherein the upper left quadrant (PI positive & annexin V negative) is neglected when evaluating necrosis, because both the common ultrasound-induced reversible sonoporation and the nanoparticle-induced reversible enhanced permeability make it difficult to differentiate dead and viable cells in this quadrant [42,43]. The upper right region herein represents necrotic cells rather than late apoptosis [44], and was taken as the research emphasis when evaluating the effectiveness of CO₂ bubbling-based

'nanobomb' system (namely, US+HMSN-LA-CO₂) in inducing cell necrosis [45]. The necrosis percentage order of these groups *via* flow cytometry: control < HMSN-LA < HMSN-LA-CO₂ < US+HMSN-LA-CO₂, is well consistent with that *via* MTT method, demonstrating CO₂ bubbling-based 'nanobomb' system induced instant necrosis of panc-1 cells. Noticeably, the decrease of necrosis percentage from 81.26% (US+HMSN-LA-CO₂) to 32.68% (HMSN-LA-CO₂) implies the cavitation effect in US+HMSN-LA-CO₂ and non-prevailing in HMSN-LA-CO₂ alone. The necrosis induced by US+HMSN-LA-CO₂ can further be confirmed *via* visual SEM imaging of panc-1 cells (Figure 5c), wherein instantaneous cell lysis, membrane collapse and necrotic disintegration after US+HMSN-LA-CO₂ treatment can be found [41, 46].

Furthermore, confocal images of panc-1 cells stained by PI & calcein after treatments with different groups also visually evidence high efficacy of US+HMSN-LA-CO₂ in inducing cell necrosis (Figure 5b). In detail, red dead cells stained by PI after US+HMSN-LA-CO₂ treatment become substantially irregular and larger, indicative of collapse and disintegration of the cells, as well as the damage or breakage of DNA chains in these collapsed cells. The similar phenomenon can also be observed in optical microscopic images (Figure S16). The schematic illustration of all *in vitro* experiments is shown in Figure 5d.

***In vivo* inertial cavitation effect of CO₂ bubbling-based 'nanobomb' system**

Before *in vivo* application, bio-distribution of CO₂ bubbling-based nanobomb (HMSN-LA-CO₂) should be investigated. It is can be found that after 8 h, the accumulative retention of HMSN-LA-CO₂ in tumor achieves the highest value (Figure S17), indicating 8 h is the optimum starting point of implementing US irradiation.

This novel CO₂ bubbling-based 'nanobomb' system was explored to inhibit *in vivo* panc-1 xenograft solid tumor. According to the photos and the volume change profiles of panc-1 tumors on tumor-bearing nude mice after treatment with different groups (Figure 6a,b), it is clear that US+HMSN-LA-CO₂, as expected, performs the best in inhibiting the growth of panc-1 tumor. From the pathological examination of H&E staining (Figure S18), the characteristic features associated with necrosis, such as collapsed cytoskeleton and nucleus disintegration can be clearly observed. During the experiments, all nude mice keep healthy according to Figure 6c, implying that neither starvation nor diseases influenced the growth of tumor.

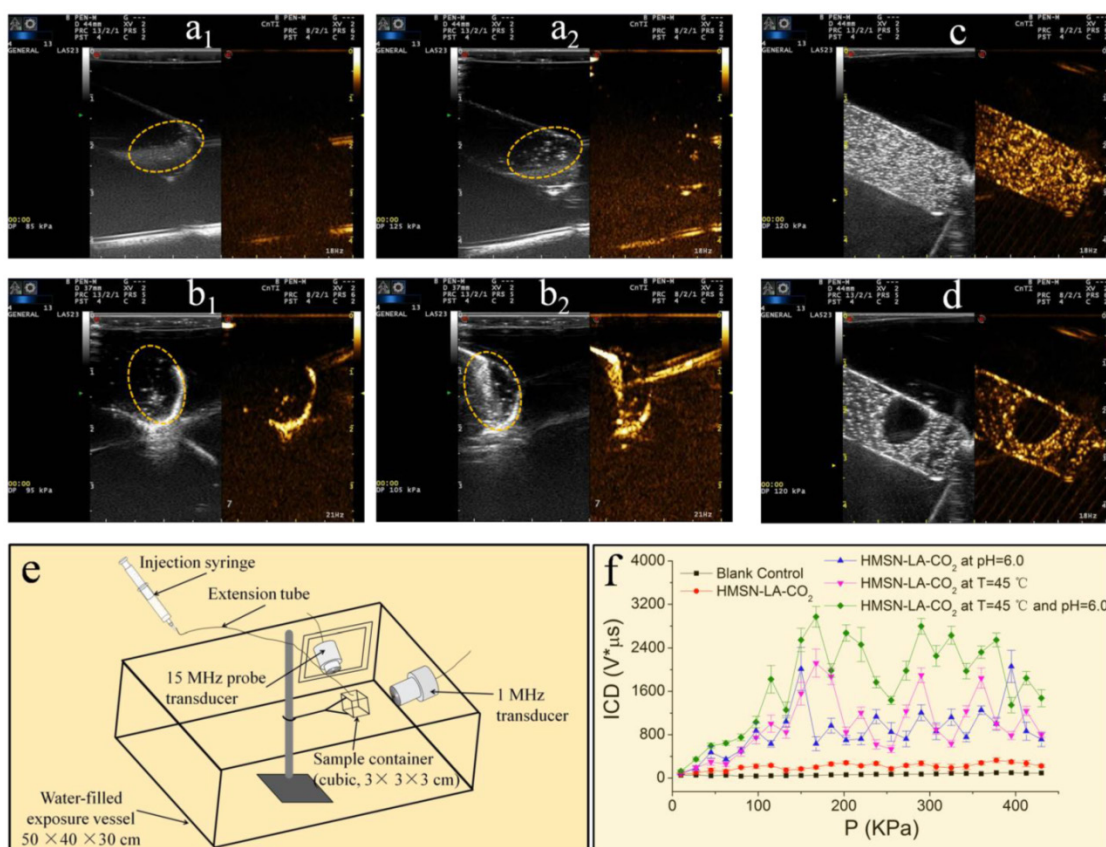


Figure 3. pH/temperature dual-responsive emergence and explosion of CO₂ bubbles from HMSN-LA-CO₂. (a) The reversible chemical adsorption equation of CO₂ by LA: (a₁,a₂) Ultrasonic images of HMSN-LA-CO₂ at 37 °C (a₁) and 50 °C (a₂) at a fixed pH = 7.4 under BFI (left) and CHI (right) modes, respectively; (b₁, b₂) Ultrasonic images of HMSN-LA-CO₂ at pH=7.4 (b₁) and 4.7 (b₂) at a fixed temperature, 37 °C under BFI (left) and CHI (right) modes, respectively. (c,d) Ultrasonic images of CO₂ bubbles obtained from HMSN-LA-CO₂ before (c) and after (d) local ultrasound irradiation under BFI (left) and CHI (right) modes, respectively. (e,f) Quantitative inertial cavitation dose (ICD) measurements: (e) schematic image of measuring system and (f) ICD values of different groups with 1 MHz transducer. Noting: BFI represents B fundamental imaging, and CHI represents contrast harmonic imaging.

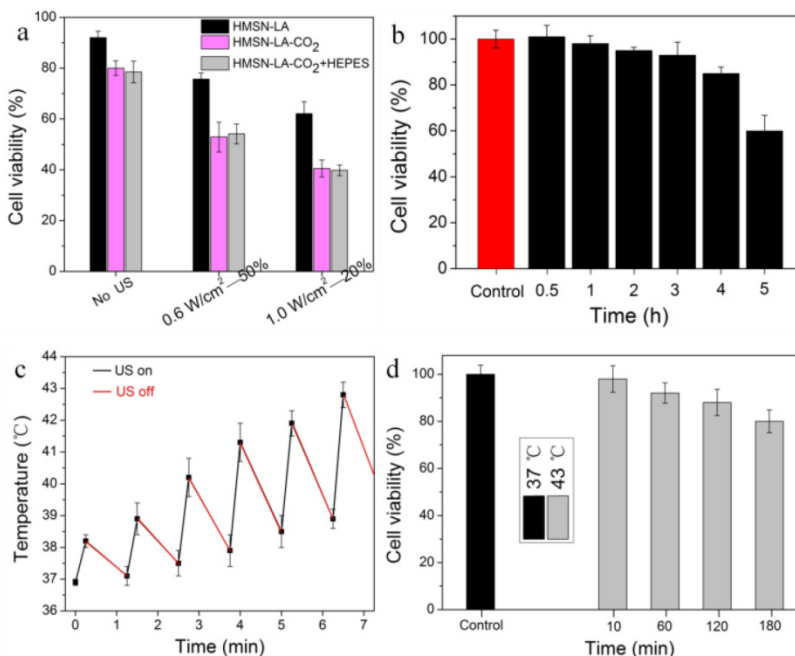


Figure 4. Exclusion of influences of pH reduction and ultrasound hyperpyrexia on cell viability. (a) Cell viability of panc-1 cells after the initial treatment with HMSN-LA, HMSN-LA-CO₂ and HMSN-LA-CO₂+HEPES and the subsequent 1.5 h incubation at 37 °C. HEPES (50 mmol/ml) was concurrently added to maintain extracellular pH at 7.2-7.3 when adding HMSN-LA-CO₂. (b) Time-dependent cell viability of panc-1 cells incubated at pH=6.2 (the pH value of CO₂ saturated solution in panc-1 culture medium at 37 °C). After different incubation periods, another 1.5 h incubation at 37 °C was carried out. (c) Temperature variation of 1640 culture medium after pulse ultrasound irradiation (1.0W/cm²-20%-122 KPa). (d) Time-dependent cell viability of panc-1 cells incubated at 37 °C and 43 °C. After different incubation period at 43 °C, another 1.5 h incubation at 37 °C was carried out, and afterwards. Noting: other parameters are that ultrasound frequency is 1 MHz, the duration time of each pulse 15 s, the interval is 60 s and the number of irradiation (cycle) is 6; and the cell viability was measured via MTT method.

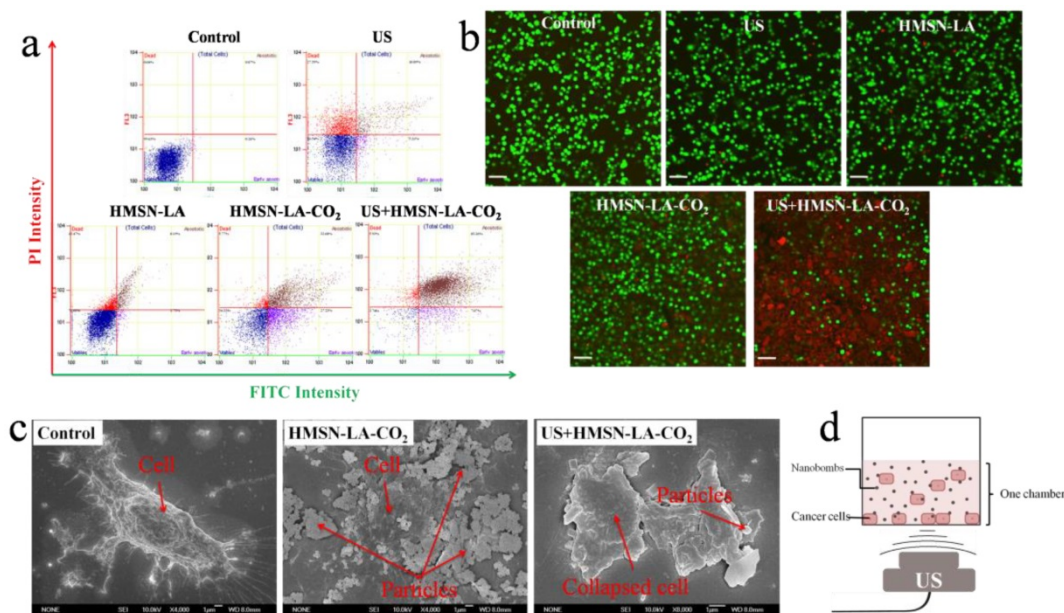


Figure 5. *In vitro* evaluations of cell death by employing the constructed CO₂ bubbling-based ‘nanobomb’ system (US+HMSN-LA-CO₂) to induce panc-1 cell necrosis. (a) Flow cytometry results of panc-1 cells treated with different groups: control, US, HMSN-LA, HMSN-LA-CO₂ and US+HMSN-LA-CO₂; (b) Laser confocal images of panc-1 cells treated with above six groups via PI & calcein double-labeling, wherein red cells (red color) were stained by PI, and viable cells (green color) were stained by calcein, and the scale bar is 60 μm; (c) SEM images of panc-1 cells after different treatments; (d) Schematics of the measurement instrument of the *in vitro* panc-1 cell experiments.

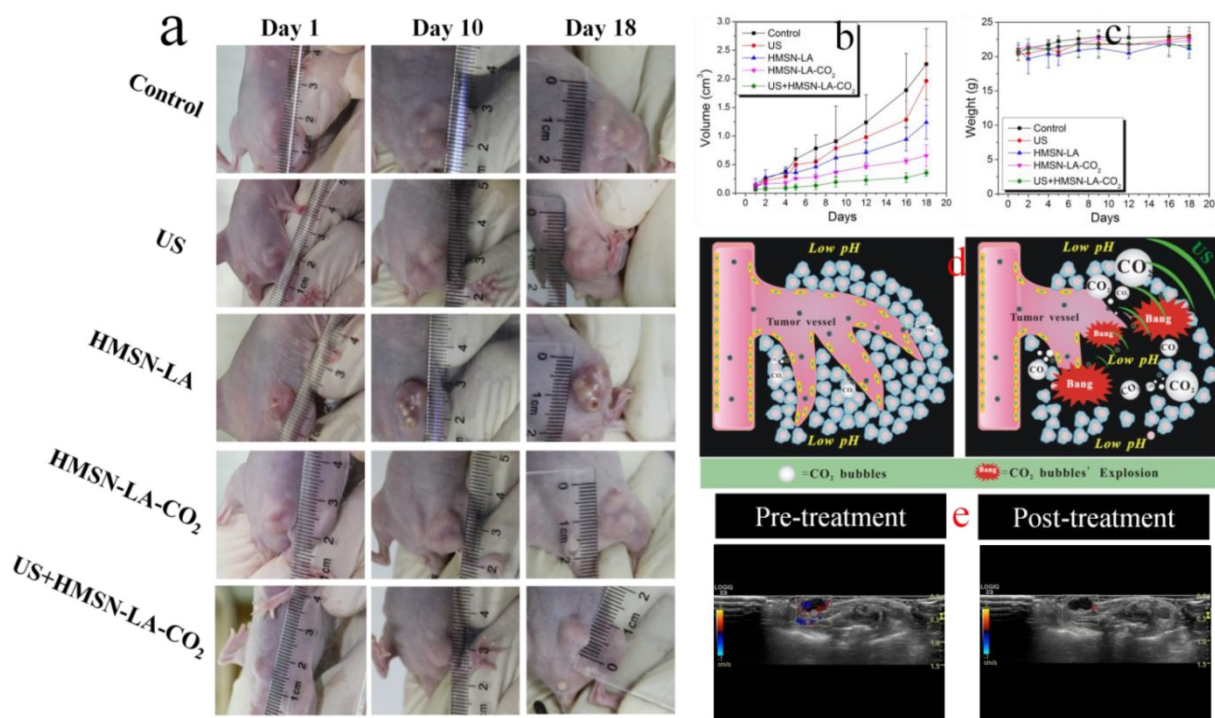


Figure 6. *In vivo* evaluations of the inhibition growth of panc-1 xenograft solid tumor by the CO₂ bubbling-based ‘nanobomb’ system (US+HMSN-LA-CO₂). (a) Digital photos of panc-1 pancreatic xenograft solid tumor after treatments with different groups at 1st day, 10th day and 18th day; (b,c) Quantitative volume variations of panc-1 pancreatic xenograft solid tumor and the body weight variations of experimental nude mice after treatments with different groups in the time course of *in vivo* experiments; (d) Technical routes of employing the constructed pH/temperature-responsive CO₂ release system to mechanically destroy vessels around panc-1 tumor and tumor cells through intravascular, intracellular and intercellular pathways via CO₂ bubbles’ cavitation effect under the triggering of ultrasound irradiation (right), in comparison with the case of no ultrasound irradiation (left), where the CO₂ bubbles induced in lower pH microenvironment in tumor will be mostly dissolved in blood or interstitial fluid, resulting in the majorly suppressed inertial cavitation (bubble explosion); (e) Color Doppler ultrasound images of panc-1 pancreatic xenograft solid tumor before (left) and after (right) treatment with US+HMSN-LA-CO₂ for 1 h, respectively.

The mechanism of US+HMSN-LA-CO₂ in inhibiting the growth of tumor (Figure 6d and Figure 2C) indicates that endogenous acidic environment in tumor and exogenous therapeutic ultrasound-induced local hyperpyrexia can cooperatively induce HMSN-LA-CO₂ to initially release CO₂ bubbles. Afterwards, the generated bubbles can enhance the EPR effect [47,48]. The enhanced EPR effect can in turn, promote more CO₂ ‘nanobombs’ to cross the blood vessels and substantially retain in the tumor tissues, thus the CO₂ nanobombs behave like ‘Trojan horse’ to react with acidic intercellular substances to release more CO₂ bubbles. These CO₂ bubbles will instantly explode to destroy tumor tissues and vessels once encountering ultrasound waves, and consequently occlude the blood supply within tumor.

To confirm this mechanism, ultrasound imaging technology was employed to monitor the blood supply and the volume variation of tumor. In the color doppler ultrasound images and videos (Figure 6e and videos S5,6), after treatment with US+HMSN-LA-CO₂ (video S5), the blood supply has been obviously occluded compared with pre-treatment (video S6), and the tumor volume become much smaller (Figure S19),

which directly demonstrates that the treatment with US+HMSN-LA-CO₂ can destroy blood vessels within tumor and inhibit the growth of tumor. Figure 7 clearly shows that the dual-responsive CO₂ release system can be well taken up by panc-1 cells (Figure 7a) and gradually accumulates in tumor *in vivo* (Figure 7b) due to the smaller size than 700 nm [49]. Especially after exposure to ultrasound irradiation, more ‘nanobomb’ can cross blood vessel *via* enhanced EPR effect induced by US irradiation and CO₂ bubbles-mediated cavitation, and retain in tumor tissue (Figure 7b), wherein more US irradiations can facilitate more retention of CO₂ bubbling-based ‘nanobomb’ in tumor. More importantly, US radiation can elevate the temperature to further promote CO₂ release from HMSN-LA-CO₂ (Figure 7c,d), which was beneficial for improving treatment efficacy of the CO₂ bubbling-based ‘nanobomb’ system. Noticeably, the maximum temperature during *in vivo* US irradiation can be controlled to be lower than 45 °C, which can maximally reduce *in vivo* temperature elevation-induced apoptosis of normal tissues adjacent to cancers, further improving treatment biosafety.

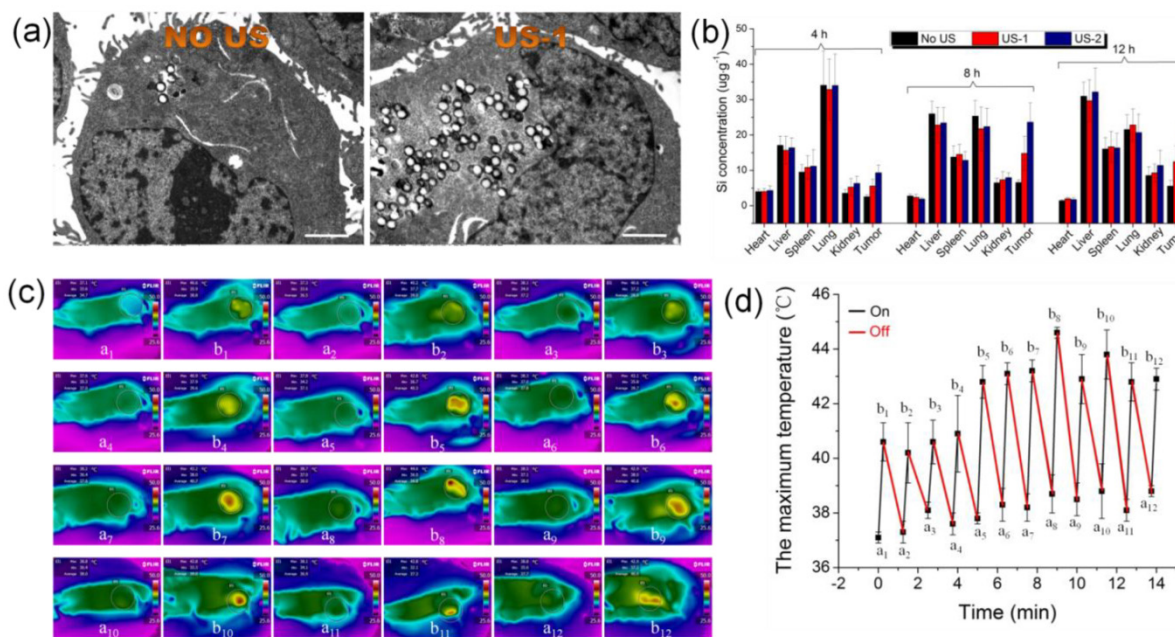


Figure 7. Ultrasound-induced enhanced uptake of HMSN-LA-CO₂ by panc-1 cells and temperature elevations *in vivo*. (a) Bio-TEM images of panc-1 cells treated with HMSN-LA-CO₂ (left) and US+HMSN-LA-CO₂ (right), respectively, scale bar: 2 μm. (b) Bio-distribution of Si element in main organs (heart, liver spleen, lung, kidney and tumor) of panc-1 pancreatic tumor-bearing nude mice treated with US+HMSN-LA-CO₂ after 4 h, 8 h and 12 h. US-1: before injecting HMSN-LA-CO₂ (0.1 ml, 15 mg/ml), the nude mice was radiated by ultrasound, and the irradiation method is pulsed (irradiation time is 15 s, the interval is 60 s and the cycle number is 6). US-2: repeated US-1 for 4 times, one occurred before injecting HMSN-LA-CO₂ and the other 3 times occurred at the beginning of each hour after injecting HMSN-LA-CO₂. (c,d) Temperature variations of panc-1 pancreatic xenograft solid tumor during pulsed ultrasound irradiation (15 s duration, 60 s interval, 20% duty cycle, 12 cycles and 1.0 W/cm² power density) *via* infrared imaging devices. (c) Thermal infrared images of temperature distributions before (a₁-a₁₂) and after (b₁-b₁₂) each cycle of ultrasound irradiation with a interval of 60 s; and (d) the maximum temperature at starting and end points of each cycle of ultrasound irradiation.

Furthermore, three molecular biology techniques, *e.g.*, the proapoptotic P53 protein and tunnel immunofluorescence staining both of which can identify apoptosis [50,51], and CD34 immunohistochemical staining that can measure the density of blood vessels (necrosis) [52], were employed. US+HMSN-LA-CO₂ treatment group acquired the lowest protein expression (Figure 8a,b) and the fewest panc-1 apoptosis (Figure 8e₁-e₅ and 8f), indicating the most excellent inhibitory capability of US+HMSN-LA-CO₂ against tumor growth derived from mechanical injury-mediated necrosis rather than apoptosis. The vascular density treated with US+HMSN-LA-CO₂ decreases to the lowest level among all the groups (Figure 8c,d), which convincingly demonstrates that the inertial cavitation deriving from US+HMSN-LA-CO₂ could mechanically de-

stroy the tumor vessels, similar to microbubbles [52,53]. It is worth noting that the treatment mechanism by HMSN-LA-CO₂ alone is majorly different from that of US+HMSN-LA-CO₂, *i.e.*, in addition to the limited necrosis by the spontaneous explosion of a few coalesced large-sized CO₂ bubbles [20], high P53 protein expression (Figure 8a,b) and tunnel-stained cells (Figure 8e₁-e₅ and 8f) indicate the presence of apoptosis in the group of HMSN-LA-CO₂ without US irradiation, as *in vitro* cytometry data shown (Figure 5a). Additionally, the cytotoxicity of HMSN-LA on normal cells, *e.g.*, L929 cell line, can be neglected (Figure S20). Nevertheless, owing to more H₂O₂ in tumor than in other normal organs reacting with LA molecules to generate NO, the HMSN-LA group also shows a certain tumor therapeutic efficacy probably via NO-mediated apoptosis [54-56].

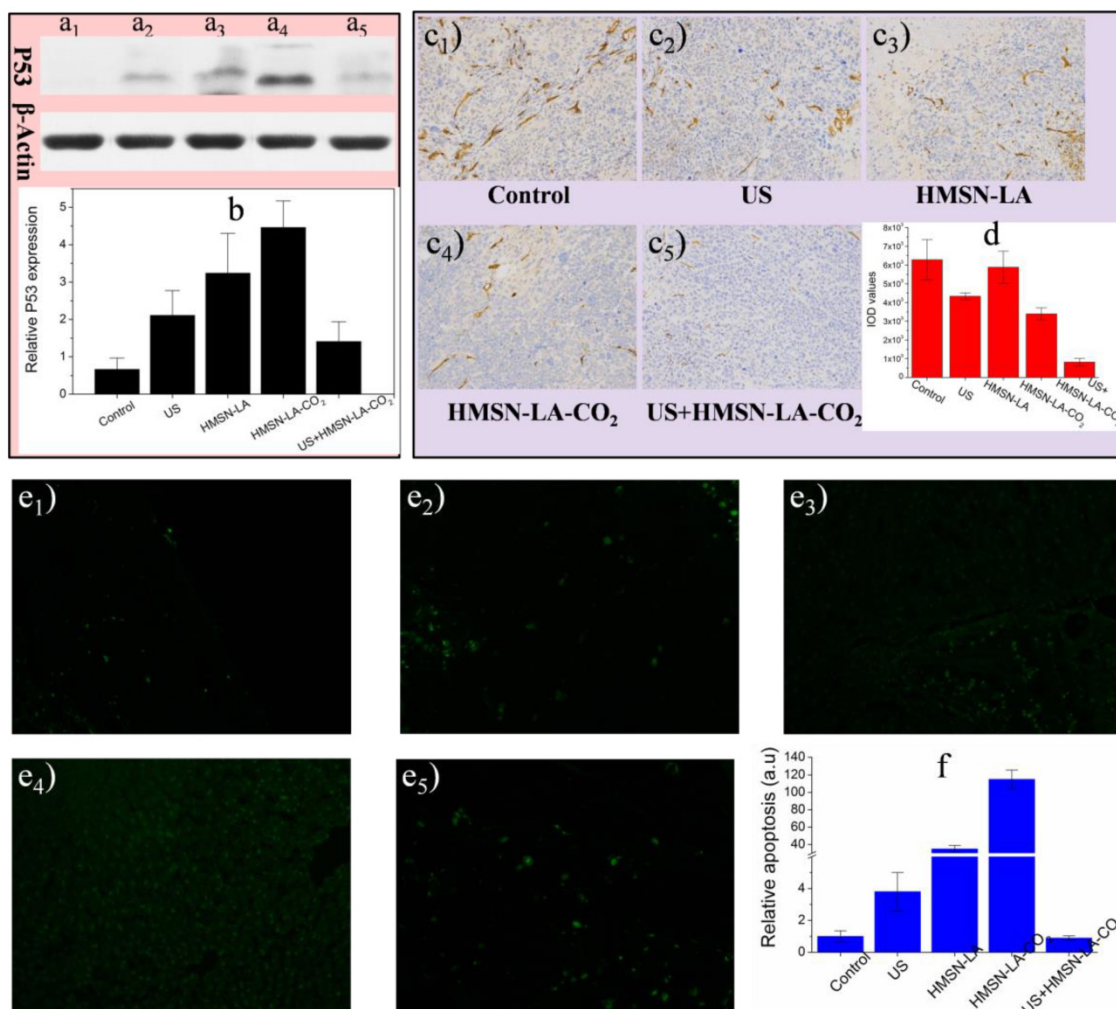


Figure 8. *In vivo* molecular biological characterizations of isolated panc-1 pancreatic xenograft solid tumor via P53 protein expression measurement, CD34 immunohistochemical staining and tunnel immunofluorescence staining. (a,b) Effects of our pH/temperature dual-responsive CO₂ nanobomb system on the expression of P53 protein determined by western blotting analysis, wherein (a) represents the protein bands of isolated panc-1 pancreatic xenograft solid tumor after treated with different groups (a₁: control, a₂: US, a₃: HMSN-LA, a₄: HMSN-LA-CO₂, a₅: US+HMSN-LA-CO₂), and (b) is the quantitative relative P53 protein expression values via comparing their corresponding gray values of P53 with standard protein, actin bands; (c,d) Effects of our pH/temperature dual-responsive CO₂ nanobomb system on destroying vessels in isolated panc-1 pancreatic xenograft solid tumor, wherein (c) shows the optical microscopic images (200-fold) of isolated panc-1 pancreatic xenograft solid tumor treated with different groups after CD34 immunohistochemical staining, and (d) gives the quantitative IOD values of the images in (c) determined by Image pro-plus 6.0 software. Notes: IOD value is positively proportional to the density of vessels. (e₁-e₅) Confocal images of apoptotic cells after treatments with different groups: control (e₁), US (e₂), HMSN-LA (e₃), HMSN-LA-CO₂ (e₄) and US+HMSN-LA-CO₂ (e₅) via tunnel immunofluorescence staining, and green represents the apoptotic cells; (f) Quantitative relative apoptosis deriving from e₁-e₅ with control group as the base.

More importantly, neither CO₂ bubbles' explosion and CO₂ bubbles' explosion-enhanced EPR effect, nor acidic intercellular substance, and nor ultrasound-induced temperature elevation is available in normal tissues, thus no evident injuries are observed *via* the HE staining (Figure S21) and CD34 immunohistochemical staining images (Figure S22), further demonstrating the biosafety of this CO₂ bubbling-based nanobomb system featured with localized treatment. In order to investigate the role of HMSNs support in this treatment process, LA-CO₂ without HMSNs support was employed for comparison. The *in vivo* results show that LA-CO₂ fails in inhibiting growth of panc-1 tumors with a much lower inhibitory effect than HMSN-LA-CO₂ (Figure S23). This phenomenon can be attributed to that without protection of HMSN supports, free LA molecules could participate in normal metabolism, *i.e.*, generating NO molecules *via* catalysis by nitric oxide synthase (NOS) to modulate normal physiological activity [55], thus could not reach to the tumor site. Therefore it is believed that the role of HMSN support is to load and protect LA molecules from leakage and helpful to safely deliver them to the tumor tissues.

Conclusions

Basing on the characteristic of reversible CO₂ adsorption/release by L-arginine, a novel type of temperature & pH dual-responsive CO₂ release system has been successfully constructed. Under the co-triggering of ultrasound irradiation and inherent acidic condition in tumor microenvironment, the CO₂ release system can release CO₂ bubbles in an on-demand manner, and explode to mechanically destroy *in vitro* panc-1 cells, and consequently induce the necrotic cell death. The *in vivo* results indicate that CO₂ bubbles' explosion from HMSN-LA-CO₂ could occlude blood supply and further greatly inhibit the growth of panc-1 solid tumor when exposed to ultrasound irradiation. More importantly, this novel treatment approach is a localized physiotherapy, which is expected to greatly reduce damages to normal organs during cancer therapy, thus leading to substantially improved efficacy and safety of tumor therapy.

Supplementary materials

Additional File 1:

Figures S1-S23.

<http://www.thno.org/v05p1291s1.pdf>

Additional File 2:

Movie S1. <http://www.thno.org/v05p1291s2.wmv>

Additional File 3:

Movie S2. <http://www.thno.org/v05p1291s3.wmv>

Additional File 4:

Movie S3. <http://www.thno.org/v05p1291s4.wmv>

Additional File 5:

Movie S4. <http://www.thno.org/v05p1291s5.wmv>

Additional File 6:

Movie S5. <http://www.thno.org/v05p1291s6.wmv>

Additional File 7:

Movie S6. <http://www.thno.org/v05p1291s7.wmv>

Acknowledgements

We greatly acknowledge financial support from the National Basic Research Program of China (973 Program, Grant No. 2011CB707905), China National Funds for Distinguished Young Scientists (51225202), National Natural Science Foundation of China (Grant No. 51072212, 81371570) and Program of Shanghai Subject Chief Scientist (Grant No.14XD1403800).

Competing Interests

The authors have declared that no competing interest exists.

References

- Moorthi C, Manavalan R, Kathiresan K. Nanotherapeutics to Overcome Conventional Cancer Chemotherapy Limitations. *J Pharm Pharmaceut Sci.* 2011; 14: 67-77.
- Wang X, Chen H, Chen Y, Ma M, Zhang K, Li F, et al. Perfluorohexane Encapsulated Mesoporous Silica Nanocapsules as Enhancement Agents for Highly Efficient High Intensity Focused Ultrasound (HIFU). *Adv Mater.* 2012; 24: 785-91.
- Wang X, Chen H, Zheng Y, Ma M, Chen Y, Zhang K, et al. Au-nanoparticle coated mesoporous silica nanocapsule-based multifunctional platform for ultrasound mediated imaging, cytolysis and tumor ablation. *Biomaterials.* 2013; 34: 2057-68.
- Chen Y, Chen H, Sun Y, Zheng Y, Zeng D, Li F, et al. Multifunctional Mesoporous Composite Nanocapsules for Highly Efficient MRI-Guided High-Intensity Focused Ultrasound Cancer Surgery. *Angew Chem Int Ed.* 2011; 50: 12505-9.
- Werner ME, Copp JA, Karve S, Cummings ND, Sukumar R, Li C, et al. Folate-Targeted Polymeric Nanoparticle Formulation of Docetaxel Is an Effective Molecularly Targeted Radiosensitizer with Efficacy Dependent on the Timing of Radiotherapy. *ACS Nano.* 2011; 5: 8990-8.
- Cutler CS, Hennkens HM, Sisay N, Huclier-markai S, Jurisson SS. Radiometals for Combined Imaging and Therapy. *Chem Rev.* 2013; 113: 858-83.
- Gao L, Fei J, Zhao J, Li H, Cui Y, Li J. Hypocrellin-Loaded Gold Nanocages with High Two-Photon Efficiency for Photothermal/Photodynamic Cancer Therapy *in Vitro*. *ACS Nano.* 2012; 6: 8030-40.
- Yang K, Xu H, Cheng L, Sun C, Wang J, Liu Z. *In Vitro* and *In Vivo* Near-Infrared Photothermal Therapy of Cancer Using Polypyrrole Organic Nanoparticles. *Adv Mater.* 2012; 24: 5586-92.
- Chen Y-w, Chen P-j, Hu S-h, Chen I-w, Chen S-y. NIR-Triggered Synergic Photo-chemothermal Therapy Delivered by Reduced Graphene Oxide / Carbon / Mesoporous Silica Nanocookies. *Adv Funct Mater.* 2014; 24: 451-9.
- Hayashi K, Nakamura M, Miki H, Ozaki S, Abe M, Matsumoto T, et al. Photostable Iodinated Silica/porphyrin Hybrid Nanoparticles with Heavy-Atom Effect for Wide-Field Photodynamic/Photothermal Therapy Using Single Light Source. *Adv Funct Mater.* 2014; 24: 503-13.
- Yuan H, Fales AM, Vo-dinh T. TAT Peptide-Functionalized Gold Nanostars: Enhanced Intracellular Delivery and Efficient NIR Photothermal Therapy Using Ultralow Irradiance. *J Am Chem Soc.* 2012; 134: 11358-61.
- Kennedy JE. High-intensity focused ultrasound in the treatment of solid tumours. *Nat Rev Cancer.* 2005; 5: 321-7.
- Mitragotri S. Healing sound: the use of ultrasound in drug delivery and other therapeutic applications. *Nat Rev Drug Discov.* 2005; 4: 255-60.
- Chung M-f, Chen K-j, Liang H-f, Liao Z-x, Chia W-t, Xia Y, et al. A Liposomal System Capable of Generating of CO₂ Bubbles to Induce Transient Cavitation, Lysosomal Rupturing, and Cell Necrosis. *Angew Chem Int Ed.* 2012; 124: 10236-40.
- Mal NK, Fujiwara M, Tanaka Y. Photocontrolled reversible release of guest molecules from coumarin- modified mesoporous silica. *Nature.* 2003; 421: 350-3.

16. Bringas E, Köysüren Ö, Quach DV, Mahmoudi M, Aznar E, Roehling JD, et al. Triggered-release in Lipid Bilayer-Capped Mesoporous Silica Nanoparticles containing SPION using an Alternating Magnetic Field. *Chem Commun.* 2012; 48: 5647-9.
17. De R, Aili D, Stevens MM. Enzyme-responsive nanoparticles for drug release and diagnostics. *Adv Drug Deliv Rev.* 2012; 64: 967-78.
18. Moon GD, Choi SW, Cai X, Li W, Cho EC, Jeong U, et al. A New Theranostic System Based on Gold Nanocages and Phase-Change Materials with Unique Features for Photoacoustic Imaging and Controlled Release-supporting. *J Am Chem Soc.* 2011; 133: 4762-5.
19. Dai J, Lin S, Cheng D, Zou S, Shuai X. Interlayer-Crosslinked Micelle with Partially Hydrated Core Showing Reduction and pH Dual Sensitivity for Pinpointed Intracellular Drug Release. *Angew Chem Int Ed.* 2011; 50: 9404-8.
20. Schutt EG, Klein DH, Mattrey RM, Riess JG. Injectable Microbubbles as Contrast Agents for Diagnostic Ultrasound Imaging : The Key Role of Perfluorochemicals. *Angew Chem Int Ed.* 2003; 42: 3218-35.
21. He Q, Shi J, Zhu M, Chen Y, Chen F. The three-stage *in vitro* degradation behavior of mesoporous silica in simulated body fluid. *Microporous Mesoporous Mat.* 2010; 131: 314-20.
22. Chen Y, Chen H, Shi J. *In Vivo* Bio-Safety Evaluations and Diagnostic/Therapeutic Applications of Chemically Designed Mesoporous Silica Nanoparticles. *Adv Mater.* 2013; 25: 3144-76.
23. Tarn D, Ashley CE, Xue M, Carnes EC, Zink JJ, Brinker CJ. Mesoporous Silica Nanoparticle Nanocarriers: Biofunctionality and Biocompatibility. *Accounts Chem Res.* 2013; 46: 792-801.
24. Tang F, Li L, Chen D. Mesoporous Silica Nanoparticles: Synthesis, Biocompatibility and Drug Delivery. *Adv Mater.* 2012; 24: 1504-34.
25. Zhang K, Chen H, Zheng Y, Chen Y, Ma M, Wang X, et al. A Facile *in-situ* Hydrophobic Layer Protected Selective Etching Strategy for the Synchronous Synthesis/Modification of Hollow or Rattle-type Silica Nanoconstructs. *J Mater Chem.* 2012; 22: 12553-61.
26. Hiyoshi N, Yogo K, Yashima T. Adsorption characteristics of carbon dioxide on organically functionalized SBA-15. *Microporous Mesoporous Mat.* 2005; 84: 357-65.
27. Zhao Y, Zhong Q. Experiment Research on CO₂ Absorption-desorption Cycles in L-Arginine Aqueous Solutions. *Proceedings of the CSEE.* 2011; 31: 84-9.
28. Liu Y, Jin L, Hou J-B, Xu P-X, Zhao Y-F. Variation in proton affinity of the guanidino group between free and blocked arginine. *Amino Acids.* 2007; 33: 145-50.
29. Vaidhyanathan R, Iremonger SS, Shimizu GKH, Boyd PG, Alavi S, Woo TK. Direct Observation and Quantification of CO₂ Binding Within an Amine-Functionalized Nanoporous Solid. *Science.* 2011; 330: 650-3.
30. Goepfert A, Czaun M, May RB, Prakash GKS, Olah GA, Narayanan SR. Carbon Dioxide Capture from the Air Using a Polyamine Based Regenerable Solid Adsorbent. *J Am Chem Soc.* 2011; 133: 20164-7.
31. Wang R, Li DF, Liang DT. Modeling of CO₂ capture by three typical amine solutions in hollow fiber membrane contactors. *Chem Eng Process.* 2004; 43: 849-56.
32. Graf C, Gao Q, Schütz J, Noufele CN, Ruan W, Posselt U, et al. Surface Functionalization of Silica Nanoparticles Supports Colloidal Stability in Physiological Media and Facilitates Internalization in Cells. *Langmuir.* 2012; 28: 7598-613.
33. Peng Y, Zheng M, Feng B, Chen X, Yu B, Lu A, et al. Hyperthermic CO₂ pneumoperitoneum induces apoptosis in human colon cancer cells through Bax-associated mitochondrial pathway. *Oncol Rep.* 2008; 19: 73-9.
34. Leng J, Lang J, Jiang Y, Liu D, Li H. Impact of different pressures and exposure times of a simulated carbon dioxide pneumoperitoneum environment on proliferation and apoptosis of human ovarian cancer cell lines. *Surg Endosc.* 2006; 20: 1556-9.
35. Park HJ, Lyons JC, Ohtsubo T, Song CW. Acidic environment causes apoptosis by increasing caspase activity. *Br J Cancer.* 1999; 80: 1892-7.
36. Nian-an H, Wen-ping W, Bei-jian H, Tao Z, Di Q. Effect of ultrasound irradiation on viability of HepG2 cell: an experimental study *in vitro*. *Technical Acoustics.* 2011; 30: 158-60.
37. Feril LB, Kondo T, Zhao Q, Ogawa R, Tachibana K, Kudo N, et al. Enhancement of Ultrasound-induced Apoptosis and Cell Lysis by Echo-contrast Agents. *Ultrasound Med Biol.* 2003; 29: 331-7.
38. Kobayashi D, Sasaki M, Watanabe N. Caspase-3 Activation Downstream from Reactive Oxygen Species in Heat-Induced Apoptosis of Pancreatic Carcinoma Cells Carrying a Mutant p53 Gene. *Pancreas.* 2001; 22: 255-60.
39. Watanabe N, Tsuji N, Kobayashi D, Yamauchi N, Akiyama S, Sasaki H, et al. Endogenous tumor necrosis factor functions as a resistant factor against hyperthermic cytotoxicity in pancreatic carcinoma cells via enhancement of the heat shock element-binding activity of heat shock factor 1. *Chemotherapy.* 1997; 43: 406-14.
40. Ashush H, Rozenszajn LA, Blass M, Barda-saad M, Azimov D, Radnay J, et al. Apoptosis Induction of Human Myeloid Leukemic Cells by Ultrasound Exposure. *Cancer Res.* 2000; 60: 1014-20.
41. Feng Y, Tian Z-m, Wan M-x, Zheng Z-b. Low intensity ultrasound-induced apoptosis in human gastric carcinoma cells. *World J Gastroenterol.* 2008; 14: 4873-9.
42. Jones J, Hallett MB, Morgan BP. Reversible cell damage by T-cell perforins. *Biochem J.* 1990; 267: 303-7.
43. Pogodin S, Werner M, Sommer J-U, Baulin VA. Nanoparticle-Induced Permeability of Lipid Membranes. *ACS Nano.* 2012; 6: 10555-61.
44. Ormerod, M. G. The study of apoptotic cells by flow cytometry. *Leukemia.* 1998; 12: 1013-25.
45. Karshafian R, Bevan PD, Williams R, Samac S, Burns PN. Sonoporation by Ultrasound-activated Microbubbles Contrast Agents: Effect of Acoustic Exposure Parameters on Cell Membrane Permeability and Cell Viability. *Ultrasound Med Biol.* 2009; 35: 847-60.
46. Lizard G, Fournel S, Genestier L, Dhedin N, Chaput C, Flacher M, et al. Revillard, Kinetics of Plasma Membrane and Mitochondria1 Alterations in Cells Undergoing Apoptosis. *Cytometry.* 1995; 21: 275-83.
47. Maeda H, Wu J, Sawa T, Matsumura Y, Hori K. Tumor vascular permeability and the EPR effect in macromolecular therapeutics: a review. *J Control Release.* 2000; 65: 271-84.
48. Lin C-Y, Tseng H-C, Shiu H-R, Wu M-F, Chou C-Y, Lin W-L. Ultrasound sonication with microbubbles disrupts blood vessels and enhances tumor treatments of anticancer nanodrug. *Int J Nanomed.* 2012; 7: 2143-52.
49. Hobbs SK, Monsky WL, Yuan F, Roberts WG, Griffith L, Torchilin VP, et al. Regulation of transport pathways in tumor vessels: role of tumor type and microenvironment. *Proc Natl Acad Sci USA.* 1998; 95: 4607-12.
50. Kawase T, Ohki R, Shibata T, Tsutsumi S, Kamimura N, Inazawa J, et al. PH Domain-Only Protein PHLDA3 Is a p53-Regulated Repressor of Ak. *Cell.* 2009; 136: 535-50.
51. Zhang C, Wu R, Zhu H, Hu Y-Z, Jiang H, Lin N-M, et al. Enhanced anti-tumor activity by the combination of TRAIL/ Apo-2L and combretastatin A-4 against human colon cancer cells via induction of apoptosis *in vitro* and *in vivo*. *Cancer Lett.* 2011; 302: 11-9.
52. Johnson CA, Sarwate S, Miller R-J, O'Brien WJr. A Temporal Study of Ultrasound Contrast Agent-Induced Changes in Capillary Density. *J Ultrasound Med.* 2010; 29: 1267-75.
53. Shen Z-Y, Shen E, Zhang J-Z, Bai W-K, Wang Y, Yang S-L, et al. Effects of low-frequency ultrasound and microbubbles on angiogenesis-associated proteins in subcutaneous tumors of nude mice. *Oncol Rep.* 2013; 30: 842-50.
54. Yang F, Chen P, He W, Gu N, Zhang X-Z, Fang K, et al. Bubble Microreactors Triggered by an Alternating Magnetic Field as Diagnostic and Therapeutic Delivery Devices. *Small.* 2010; 6: 1300-5.
55. Carpenter, A.W.; Schoenfish, M.H. Nitric oxide release: Part II. Therapeutic applications. *Chem Soc Rev.* 2012; 41: 3742-52.
56. Szatrowski PC, Nathan CF. Production of large amounts of hydrogen peroxide by human tumor cells. *Cancer Res.* 1991; 51: 794-8